ADVANCED MATERIALS TECHNOLOGIES
www.advmattechnol.de

A Digital-to-Channel Microfluidic Interface via Inkjet Printing of Silver and UV Curing of Thiol–Enes

*Gowtham Sathyanarayanan, Markus Haapala, Christopher Dixon, Aaron R. Wheeler, and Tiina M. Sikanen**

Microfluidic sample manipulation is a key enabler in modern chemical biology research. Both discrete droplet-based digital microfluidic (DMF) assays and continuous flow in-channel assays are well established, each featuring unique advantages from the viewpoint of automation and parallelization. However, there are marked differences in the applicable microfabrication materials and methods, which limit the interfacing of DMF sample preparation with in-channel separation systems, such as the gold standard microchip electrophoresis. Simultaneously, there is an increasing demand for low-cost and user-friendly manufacturing techniques to foster the adaptation of microfluidic technology in routine laboratory analyses. This work demonstrates integration of DMF with in-channel separation systems using only low-cost and accessible (non-cleanroom) manufacturing techniques, i.e., inkjet printing of silver for patterning of the driving electrodes and UV curing of off-stoichiometric thiol–ene (OSTE) polymers both for dielectric coating of the electrode arrays and replica molding of the microchannel network. As a dielectric, OSTE performs similar to Parylene C (a gold standard dielectric in electrowetting), whereas its tunable surface and bulk properties facilitate straightforward bonding of the microchannel with the dielectric layer. In addition, a new chip design that facilitates efficient droplet transfer from the DMF part to the microchannel inlet solely by electrowetting is showcased.

1. Introduction

Digital microfluidics (DMF) is an automated microscale liquid handling technique with the ability to manipulate picoliter- to microliter-sized droplets in parallel on an array of insulated driving electrodes using electrostatic forces.[1] With automated droplet actuation,[2] multiple individual droplets can be dispensed, mixed, and split in parallel to perform sequential sample manipulation protocols, such as rinsing, preconcentration, reaction, and extraction. Interfacing of DMF with a range of optical,[3,4] electrochemical,[5–7] and mass spectrometric detection[8–11] methods is well established and the fabrication of the devices has already been pushed toward low-cost cleanroom-free techniques.[12,13] As a result, DMF is a robust and cost-effective technology for miniaturization of various biochemical assays including but not limited to immunological,[14] enzymatic,[15] cell-based,[16] PCR,[17] drug,[18] and biopsy[19] screening assays. However, in some instances, the specificity of direct in situ detection may not be sufficient to distinguish multiple sample components from each other, and in these cases, the droplet must be transferred for further analysis into on-chip or off-chip chemical separation systems. To date, much of the prior work has exploited off-chip analysis of DMF-manipulated samples, which is however relatively complicated and prone to sample losses during the droplet transfer from micro- to macroscale. Although a variety of miniaturized electrophoretic and chromatographic separation chips have been reported in general,[20–22] their integration with DMF has not been comprehensively established, likely because of the marked differences in the applicable microfabrication materials and methods.

DMF driving electrodes are typically defined on a glass substrate by photolithography. Recently, increasing effort has been put into

G. Sathyanarayanan, Dr. M. Haapala, Dr. T. M. Sikanen
Faculty of Pharmacy
Drug Research Program
Division of Pharmaceutical Chemistry and Technology
University of Helsinki
P. O. Box 56, Helsinki FI-00014, Finland
E-mail: tiina.sikanen@helsinki.fi

The ORCID identification number(s) for the author(s) of this article can be found under https://doi.org/10.1002/admt.202000451.

DOI: 10.1002/admt.202000451

Dr. C. Dixon, Prof. A. R. Wheeler
Department of Chemistry
University of Toronto
80. St. George Street, Toronto, Ontario M5S 3H6, Canada
Prof. A. R. Wheeler
Donnelly Centre for Cellular and Biomolecular Research
University of Toronto
160 College, Street, Toronto, Ontario M5S 3E1, Canada
Prof. A. R. Wheeler
Institute for Biomaterials and Biomedical Engineering
University of Toronto
164 College, Street, Toronto, Ontario M5S 3G9, Canada

fabrication of electrodes by rapid inkjet prototyping techniques[11] as well as by using mass manufacturing techniques, such as printed circuit board (PCB) processing[23] or microcontact printing.[24] The dielectric coating typically relies on chemical vapor deposition (CVD) of Parylene C because its deposition quality is often superior (defect-free) compared with, for instance, spin-coated dielectric layers. However, Parylene C does not readily support monolithic integration (adhesion) of subsequent microfluidic layers, and with a view to mass manufacturing, CVD is inherently a batch process. In previous work, Parylene C based DMF devices have been combined with microchannel networks, e.g., by adhesive bonding a poly(dimethyl siloxane) (PDMS)-based channel on top of the DMF bottom plate[25,26] or by drilling a through-hole to the DMF bottom plate, which facilitates droplet transfer from the electrode array into a microchannel etched in glass underneath the electrodes.[27] However, both of these approaches have limitations. For example, although easy to bond, PDMS suffers from substantial nonspecific surface interactions (biofouling). Glass instead has more favorable surface properties (less biofouling), but micromachining of glass is technically demanding and time consuming. From this perspective, UV-curable polymers, such as lithographically defined SU-8, appear as appealing alternatives as they enable fabrication of both the dielectric layer[11] and the microfluidic channel[28] by photolithography, and are transferable to mass manufacturing processes, such as roll-to-roll production.[29] However, sealing of SU-8 microstructures with additional SU-8 layers requires specialty bonding processes,[30] which are commonly overcome by the use of a PDMS sealing layer instead (with the aforementioned biofouling issues).[28] Moreover, although channels composed of multiple materials may suffice for many microfluidic operations (e.g., droplet microfluidics), in chemical analysis (e.g., by microchip capillary electrophoresis (MCE)), the mixed material channels induce significant band broadening (loss of separation efficiency) due to nonuniform surface charge and undesirable interactions.[31] Thus, the ideal material for a DMF-to-channel interface should form both the dielectric layer and microchannel structures, enabling both patterning and effective bonding of the microchannel.

Here we developed a new non-cleanroom microfabrication approach to modular integration of channel microfluidics with DMF by exploiting low-cost inkjet printing for patterning of the driving electrodes and UV curing of thiol–enes for fabrication of the dielectric and microfluidic layers. Our chip design incorporates fully integrated electrodes for performing microchip capillary electrophoresis as well as DMF sample preparation in an automated fashion. With respect to performance characterization, we addressed three critical aspects of successful digital-to-channel microfluidic integration, including the use and characterization of off-stoichiometric thiol–enes (OSTE) as new dielectrics for DMF, droplet transfer from DMF to the microchannel inlet, and leakage-free bonding of the microchannel layer to the dielectric layer (with a view to DMF interfacing with MCE).

2. Results and Discussion

2.1. Microchip Material and Design Considerations

With a view to mass manufacturing of DMF devices, benchtop inkjet printers provide a cost-efficient approach to rapid prototyping and design optimization of DMF devices using microfabrication materials that are considerably well transferable to high-throughput manufacturing processes (e.g., roll-to-roll printing). In this study, the electrode arrays for both DMF and MCE were fabricated by inkjet printing of silver nanoparticles on a commercial mesoporous and flexible substrate (Novele IJ-220), which has been shown to provide a robust platform for manufacturing of low-cost DMF devices.[12] In previous studies[25,27] involving hybrid devices that feature DMF sample preparation upstream of MCE separations, external platinum electrodes were required to be manually inserted into the inlets and outlets of the MCE chip. These previous methods are suitable for prototypes but are not scalable for mass manufacturing. This motivated our development of all-printed electrode arrays to support all of the DMF and MCE operations (**Figure 1**a). The printed electrodes were spin-coated with OSTE (Figure 1b), which served as a dielectric material and enabled exposure of the contact pads by photolithography (Figure 1c) as well as subsequent bonding of a replica-molded microchannel (also made of OSTE) onto the dielectric (Figure 1d). The ground potential for DMF was provided by affixing a flexible, indium-tin-oxide-coated polyethylene terephthalate (ITO-PET) film on top of the DMF part of the chip (Figure 1d). Before use, the top and bottom (DMF part) plates were further spin-coated with FluoroPel and affixed to glass support plates (Figure 1d).

In principle, any nonconducting material could serve a DMF dielectric, and a number of such materials have been tested, ranging from common dielectrics processed in the cleanroom (such as Parylene C) to more unorthodox materials such as sandwich wrap[32] and plant leaves.[33] Apart from these proof-of-concept reports, most researchers choose to use Parylene C, which is formed via CVD, usually in a cleanroom environment to avoid contamination. As Parylene C features a modest dielectric constant of $\varepsilon_{par} = 3.1$, it is not preferred for its dielectric properties, but rather for its high resistance to dielectric breakdown and the straightforward process used to form highly homogenous coatings with no pinhole defects—which would render devices inoperable. In this study, to facilitate subsequent integration of microfluidic channels with the DMF device, we examined the compatibility of UV-curable and spin-coatable polymers (SU-8 and OSTE) as alternative dielectric materials for inkjet-printed DMF devices. It was observed that compared with the commonly used SU-8, OSTE polymers were more reliable for coating of mesoporous printing media and provided much better surface quality with respect to both DMF actuation and bonding of the microchannel layer (**Figure 2**). The surface roughness (arithmetic averages of the absolute values of the profile height deviations from the mean line) of SU-8 and OSTE layers, when coated onto the Novele printing media, were 5.3 and 0.76 μm, respectively. We suspect that the relatively poor quality of SU-8 coatings was a result of material reflow into the pores of the substrate during soft bake (i.e., evaporation of the solvent), which created a heterogeneous and uneven surface (Figure 2c,e). With solvent-free OSTE, this type of reflow effect was completely avoided and smooth surfaces were obtained (Figure 2d,f), which was critical to facilitating straightforward bonding of the OSTE microchannel layer on top of the dielectric layer.[34] In this study, an allyl-rich OSTE composition was used for the construction of the integrated DMF–microchannel devices, because of its improved properties (less nonspecific interactions, more stable surface charge) relative

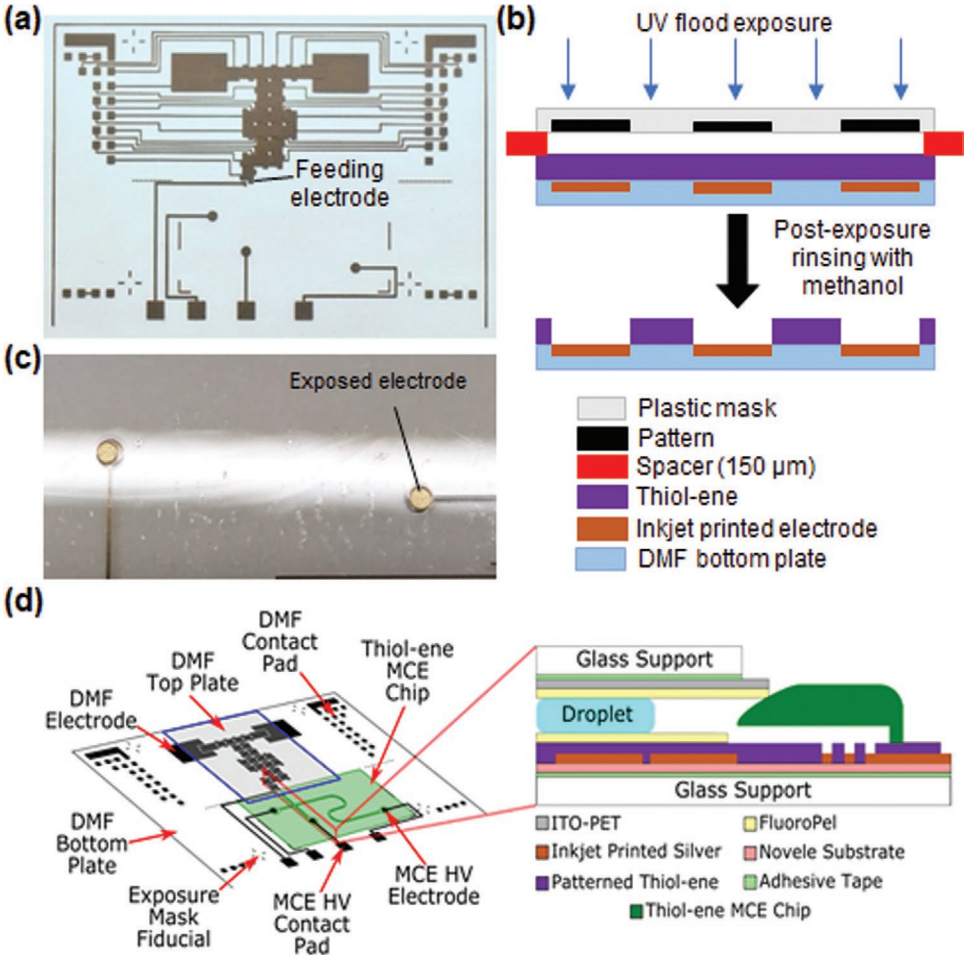

Figure 1. Hybrid DMF–MCE devices formed by inkjet printing of silver and photopatternable OSTE polymers. a) Photograph of printed electrodes on Novele substrate. Note the feeding electrode at the interface between the digital and microchannel parts of the device. b) Side-view illustration of the OSTE coating (purple) on printed electrodes (brown) and their masked exposure. c) Photograph of the exposed electrodes (diameter 1.6 mm) on OSTE coated bottom plate. (The white horizontal line is a reflection from a light source.) d) Isometric schematic view of the complete integrated DMF–microchannel device featuring inkjet-printed DMF and MCE driving electrodes, spin-coated OSTE dielectric and fluoropolymer layers, replica-molded OSTE microchannel (green) bonded onto the dielectric, and ITO-PET top plate. Call-out: cross-section illustration of the two-plate DMF–microchannel interface (illustrations are not to scale).

to thiol-rich compositions for MCE applications.[35] The materials cost of a fully assembled digital-to-channel microfluidic device, including the adhesive tape and the support glass substrates, was $1.34 (USD), and the price of the disposable parts only, without the supporting structures, as little as $0.74 (USD) (Table S1, Supporting Information). A batch of eight fully integrated devices could be fabricated in ≈120 min (Table S2, Supporting Information). However, much of the time went to MCE channel fabrication, which can be parallelized with the DMF (top and bottom plate) fabrication, and to one-by-one spin-coating of the inkjet-printed devices, which is easy to scale-up by adapting, for instance, roll-to-roll polymer coating techniques to the chip fabrication.

2.2. Dielectric Performance of OSTE Coatings

In the existing literature,[36] thiol–ene click chemistry has been postulated to have good material stability (due to high crosslinking degree) and excellent insulating properties with relative permittivity of ε_{TE} = 5.1. Further, thiol–ene polymers have been previously used as the dielectric material in electronic applications, namely in organic thin-film transistors.[36] To evaluate the feasibility of OSTE polymers for use as a dielectric for DMF, we studied the velocity of actuated droplets, which is a suitable metric for evaluating device performance as it is a function of both driving and resistive forces that counter droplet movement.[37] Droplet velocities can be measured easily using the capacitance feedback feature of the open-source DroptBot control system.[2] The dielectric performances of three different thiol–ene formulations, including allyl-rich, thiol-rich, and stoichiometric thiol–ene bulk compositions, were examined and compared with that of vapor deposited Parylene C, the "gold-standard" dielectric for DMF applications. In these tests, all bottom plates were inkjet-printed as described in Figure 1, whereas the top-plates were composed of ITO-coated glass plates spin-coated with FluoroPel. The performances of both stoichiometric thiol–ene and OSTE compositions compared well with that of Parylene C with respect to both droplet velocities (**Figure 3**a) and longevity of movement (Figure 3b).

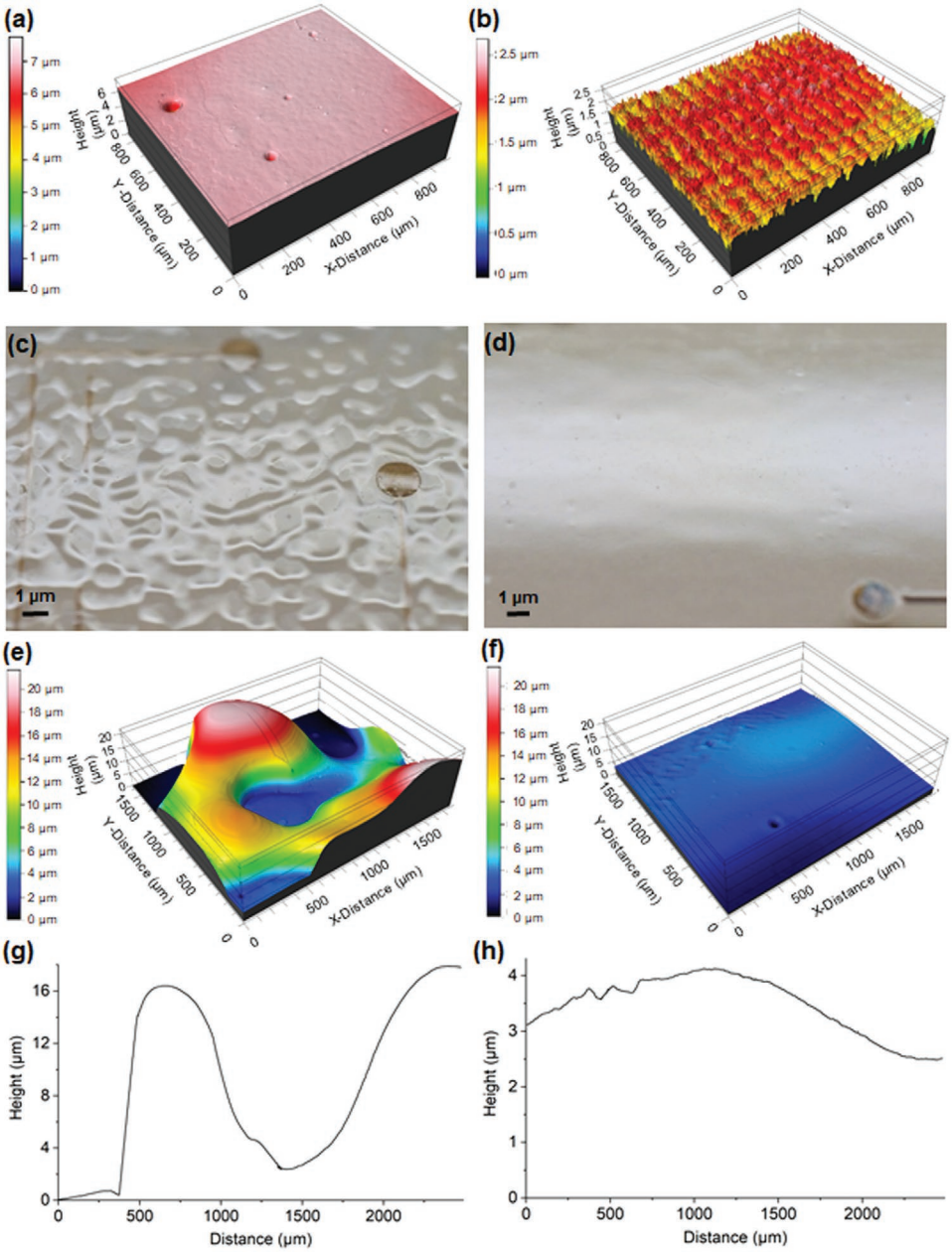

Figure 2. Dielectric coatings. 3D profilometer images of a) bare Novele substrate, b) inkjet-printed silver on Novele, and c) SU-8 spin-coated, soft baked and cured on Novele, and d) OSTE spin-coated and cured on Novele. e,f) 3D profilometer images and g,h) diagonal line plots of the surface roughness of SU-8 spin-coated, soft baked and cured on Novele (e,g) and OSTE spin-coated and cured on Novele (f,h).

A close examination of the data suggests that at any given force, the droplet velocities are highest for allyl-rich formulations followed by stoichiometric and thiol-rich compositions. This suggests that the threshold forces (i.e., the forces required to start droplet movement) are larger for TE dielectrics that contain a greater proportion of thiol functional groups. Thin fluoropolymer coatings for DMF (e.g., the FluoroPel used here), are known to be porous,[38] and it is typically assumed that liquids make physical contact with the dielectric material. Materials featuring a larger proportion of thiol groups could be expected to form more hydrogen bonds (as electron donors and/or acceptors[39]) with water molecules, which might explain the need for a higher driving force for a given velocity on such surfaces. While the relatively small variances in droplet velocity are interesting, the most practical aspect of the dielectric material is its stability over long-term use. Figure 3b indicates that all of the dielectrics tested showed somewhat constant velocities over 10 min of continuous actuation of droplets—indicating that OSTE dielectrics would be suitable for the complex, multistep assays that are often performed using DMF. On the other hand, the fact that the performances do not vary greatly between the different compositions enables substantial

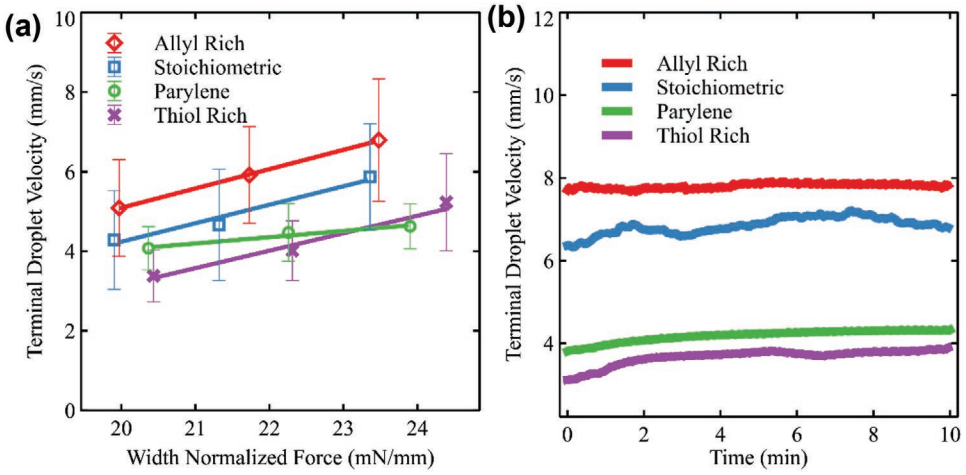

Figure 3. Thiol–ene dielectric performance characterization. a) Force–velocity and b) time–velocity plots comparing identical droplets actuated on conventional Parylene C dielectric (green), allyl-rich OSTE dielectric (red), thiol-rich OSTE dielectric (blue), and stoichiometric thiol–ene dielectric (purple). Error bars represent ±1 standard deviation for at least three droplets evaluated on two different devices (each material composition).

flexibility in the device design as the user may tune the molar ratio of thiol and allyl monomers, and thus the materials properties on demand. For example, one of the most appealing features of OSTE polymers is their tunable surface chemistry (free thiol or allyl functional groups), which has facilitated versatile biofunctionalization protocols on OSTE-based microchannel devices.[15,40,41] Besides surface properties, mechanical properties may also be manipulated by tuning the ratio of thiol and allyl monomers,[42] which is critical with a view to translation of the rapid prototyping processes onto mass manufacturing basis, e.g., by roll-to-roll printing.[43]

2.3. Digital-to-Channel Microfluidics Integration

A critical challenge for hybrid digital–channel methods are the mechanics of delivering samples from DMF part to the microchannel part of the device. For effective transfer of droplets, we designed a custom interface using an ITO-PET film as the top plate (instead of commonly used rigid ITO-coated glass plates). The ITO-PET sheet was flexible enough to bend and rest on top of the curved edge of the MCE microchannel bonded next to the DMF electrode array (Figure 1d), so that when the droplet was brought from the DMF part to the proximity of the microchannel inlet, it was continuously in contact with ground (top plate) until it reached the hydrophilic inlet and wetted the microchannel by capillary forces (**Figure 4**a). Part of the feeding electrode was also left uncoated to increase hydrophilic attraction of the droplet from the DMF part to the microchannel inlet after it reached the interface. To avoid the spreading of the droplet around the inlet, hydrophobic barriers were defined with wax around the inlet and onto the MCE microchannel edges facing the DMF part. The efficiency of the droplet transfer using this configuration is visualized with a drop of water, dyed with blue food colorant and containing 0.1% F-68 as the surfactant (Video S1, Supporting Information).

A final and critical challenge for digital-to-channel devices is whether the combination of the two modalities is detrimental to the quality of bonding between the microchannel and DMF surfaces. This was assured with the help of MCE as bonding quality corresponds with the reproducibility and profile (width and symmetry) of repeated injections of sample into the separation channel. The allyl-rich OSTE composition was selected for the MCE partly due to its favorable surface properties, i.e., high electroosmotic flow and reduced nonspecific interactions compared to other thiol–ene formulations, along with its desirable performance as a DMF dielectric (Figure 3). For the assessment of bonding quality, the microchannel was prefilled with the run buffer and the sample droplet was electrokinetically loaded from the inlet into the microchannel network, where the analyte was injected. A series of MCE runs were performed by injecting 5 µm Oregon green through a double-T injector, and the profile of the injected sample zone was monitored by epifluorescence microscopy (Figure 4c,d). The characteristic performance parameters of the injections provided evidence that there was no substantial peak broadening due to sample spreading between the bonded OSTE layers (Figure 4e). Specifically, the peak widths were narrow (1.3 ± 0.2 s, 13% RSD, $n = 4$ repeated injections), the migration time repeatability was good (3.8% RSD), and the number of theoretical plates high ($\approx 6 \times 10^4$ m^{-1}), which are comparable with variabilities reported previously[25,27] for DMF–channel interfaces: 1.6–8.4% in peak size, and 1.0–2.1% in migration time[25,27] Most importantly, when compared to previously reported DMF–MCE configurations, the inkjet-printed MCE electrodes also represent an advance in that the fabrication of this new system is fully upscalable, as all of the electrodes (DMF and MCE) are integrated and located on the same plane. Besides straightforward fabrication, this allows for facile connections to the HV power supply and the DropBot system.

3. Conclusion

In this study, we introduced OSTE polymers for low-cost, noncleanroom microfabrication of integrated digital-to-channel

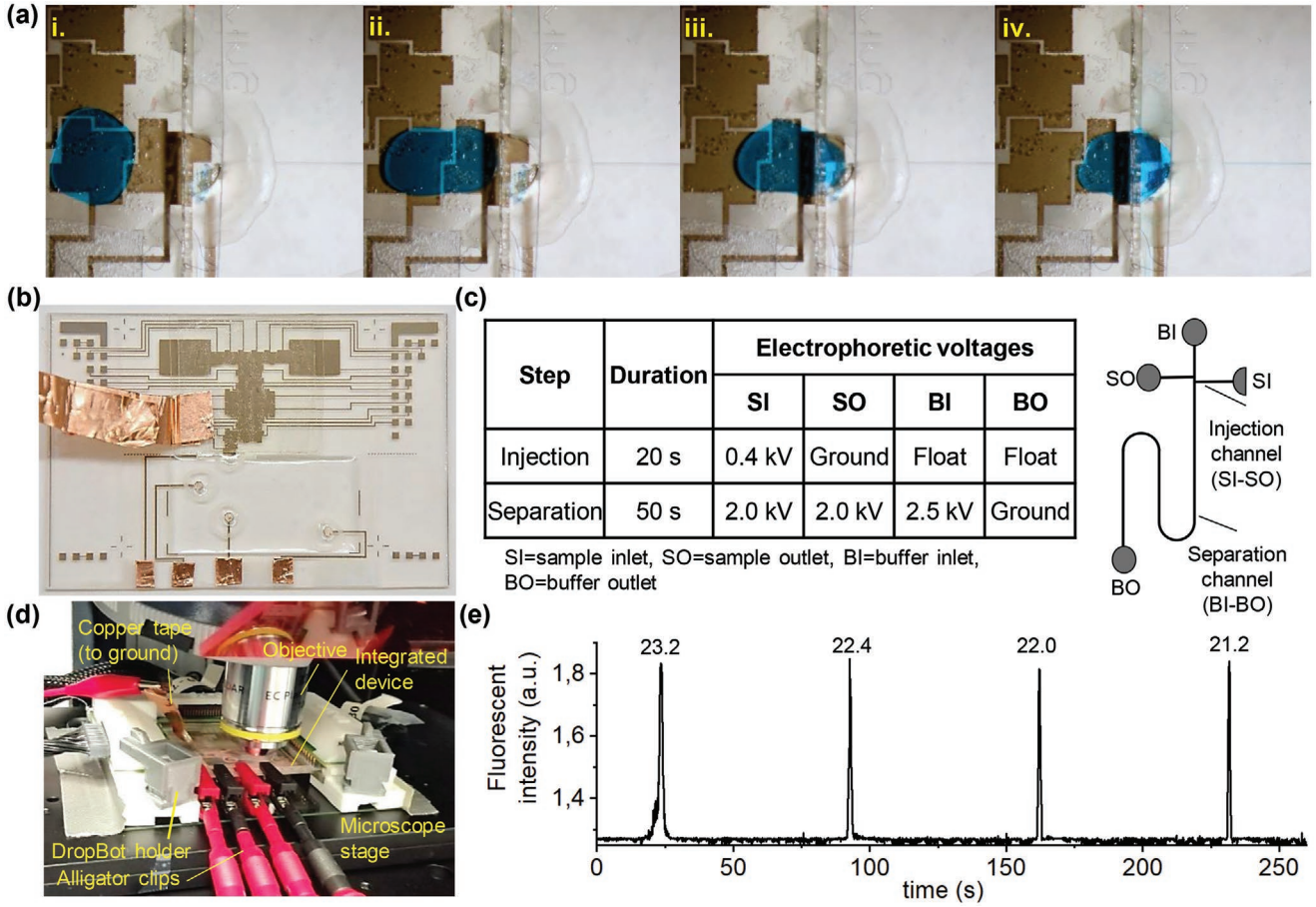

Figure 4. Digital–channel interface and electrophoretic analysis. a) Snapshots of a video visualizing the delivery of a blue food color droplet (in water) from the DMF part to the microchannel part of the device: i,ii) actuation of the droplet with DMF toward the microchannel inlet; iii) spontaneous filling of the microchannel inlet; iv) filling of the microchannel by capillary forces. b) Photograph of the fully assembled integrated DMF–microchannel device. c) Schematic presentation of the MCE channel and voltages used for verification of bonding by MCE, featuring the durations and electrical potentials applied to SI, SO, BI, and BO. d) Photograph of the MCE setup under upright epifluorescence microscope. e) Fluorescent signals of four consecutive injections of 5×10^{-6} M Oregon Green in sodium borate buffer (20×10^{-3} M, pH 10.0) using voltages given in (c). Times on top of the peaks refer to migration times (from injection cross to point of detection). The fronting of the first peak is associated with positive pressure pulse (toward the injection cross) caused by the droplet introduction to the sample inlet, which may result in minor sample leaking into the separation channel before the voltage sequence has been switched on.

microfluidic devices on mesoporous and flexible printing media incorporating the driving and MCE electrodes. The OSTE polymers were used both as the dielectric material as well as the material of choice for replica molding of microchannels so that these could be bonded with the dielectric layer to yield all-OSTE devices. As the dielectric material, all OSTE compositions tested yielded smooth surfaces and performed similarly to the current gold-standard dielectric, Parylene C. In addition, the microchannels integrated with the DMF devices met the key performance criteria of MCE, with no observations of problems with bonding quality or unevenness of the surfaces. Finally, all microfabrication materials and the methods reported here are compatible with mass manufacturing techniques, such as roll-to-roll production of printed electronics and polymer microfluidics, thus facilitating not only rapid prototyping of new designs in standard laboratory conditions, but also upscaling of the developed prototypes for high-volume production.

4. Experimental Section

Microfabrication Materials: Novele IJ-220 printing media, empty ink cartridges, Metalon JS-B25P silver nanoparticle ink, and Metalon Aqueous Vehicle (solvent) were purchased from NovaCentrix (Austin, TX). ITO-PET film was purchased from MEMCON Ltd. (Stevensville, MI). Silver conductive paint was purchased from Electrolube (Leicestershire, UK) and beeswax was purchased from Hobby Point (Helsinki, Finland). 1,3,5-Triallyl-1,3,5-triazine-2,4,6(1H,3H,5H)-trione, 98% (triallyl) was purchased from Sigma-Aldrich (Steinheim, Germany) and pentaerythritol tetrakis(3-mercaptopropionate) (tetrathiol) was purchased from Bruno Bock Chemische Fabrik GmbH & Co. KG (Marschacht, Germany). Irgacure TPO-L (photoinitiator) was kindly donated by BASF (Ludwigshafen, Germany). SU-8 25, SU-8 100, and SU-8 developer were purchased from Microchem Corp. (Westborough, MA). Sylgard 184 poly(dimethylsiloxane) (PDMS) was purchased from Dow Chemical Company (Midland, MI). Fluoropolymer FluoroPel PFC 1604V and PFC 110 fluorosolvent were purchased from Cytonix LLC (Beltsville, MD) and methanol and isopropanol were purchased from Honeywell Specialty Chemicals GmbH (Seelze, Germany). Microscope slides of the size 76 mm × 52 mm ($w \times l$) were purchased from Paul Marienfeld GmbH & Co. KG (Lauda-Königshofen,

Germany) and microscope glass slides of the size 76 mm × 26 mm were purchased from Thermo Fisher Scientific (Waltham, MA). Test grade 100 mm silicon wafers were purchased from Siegert Wafer (Aachen, Germany). Double-sided Scotch tape and adhesive transfer tape F9460PC were purchased from 3M Company (Maplewood, MN).

Chemicals and Reagents: Pluronic F-68, sodium dodecyl sulfate (SDS), and sodium hydroxide were purchased from Sigma-Aldrich, boric acid from Riedel-de Haen (Seelze, Germany), and Oregon green was purchased from Invitrogen (Carlsbad, CA). Water was purified with a Milli-Q water purification system (Merck Millipore, Molsheim, France). Tetronic 90R4 (BASF Corp., Ludwigshafen, Germany) was generously donated by Brenntag Canada (Toronto, ON). All solvents were of analytical or HPLC grade.

Fabrication of the Inkjet-Printed Digital Microfluidic Chip: DMF bottom plates were fabricated by inkjet printing of silver nanoparticle ink onto a commercial mesoporous and flexible substrate (Novele IJ-220 printing media, thickness 140 ± 12 µm) by using an Epson C88+ inkjet printer (Seiko Epson Corporation, Suwa, Japan) using methods similar to previous reports.[12] The electrode array design featured 22 roughly square interdigitated driving electrodes (2.8 mm × 2.8 mm), two reservoir electrodes (9.8 mm × 6.6 mm), and two dispensing electrodes (5.2 mm × 2.4 mm) (Figure 1a). The electrode at the interface between DMF and microchannel regions of the dice was deemed the feeding electrode. The gaps between adjacent electrodes as well as the widths of the traces connecting driving electrodes to contact pads were both designed to be 150 µm. The array also featured three circular MCE electrodes (r = 0.8 mm) and a single quarter-circle MCE electrode (r = 0.7 mm) for the application of electrokinetic flow in the microchannel part of the device (Figure 1a). The width of the traces connecting these electrodes to contact pads was designed to be 280 µm. After inkjet printing, the metallized substrates were individually affixed onto glass support plates (76 mm × 52 mm) with adhesive transfer tape. The dielectric layer was formed by CVD deposition of Parylene C as described previously[12] (control devices) or prepared from tetrathiol and triallyl monomers mixed in a molar ratio of either 125:100, 100:100, or 100:125 (thiol:allyl functional groups) containing 0.1% TPO-L as the photoinitiator. For the OSTE devices, the monomer mixture was spin-coated (3000 rpm, 30 s) onto the inkjet-printed DMF devices and cured by UV illumination (Dymax 5000-EC flood exposure lamp, Dymax Corporation, Torrington, CT; nominal intensity 225 mW cm^{-2}) in noncontact mode with 0.15 mm spacers between the photomask and the spin-coated OSTE layer (Figure 1b). Masked exposure was used to open through-holes in the OSTE layer to the contact pads (Figure 1c). Development (rinsing of uncured thiol–ene) was performed with methanol followed by drying with nitrogen gas. The resulting thickness of the thiol–ene dielectric layer was ≈5 µm. Finally, 1% FluoroPel PFC was spin-coated (1200 rpm, 30 s) on top of the dielectric and baked (150 °C, 15 min). During spin-coating (but not baking), the microchannel part of the device and the tip of the feeding electrode were protected by Parafilm. To increase the durability of the electrodes, conductive silver paint was applied onto the MCE electrodes before bonding of the microchannel layer. The top plate of the DMF device (Figure 1d) was an ITO-PET film (≈30 mm × 30 mm) affixed onto a glass slide (76 mm × 26 mm) with adhesive transfer tape, spin-coated (1500 rpm, 30 s) with 1% FluorePel PFC, and baked (150 °C, 15 min).

Integration of Channel Microfluidics with Thiol–Ene-Based Digital Microfluidic Platforms: The microchannel part of the integrated device was fabricated out of tetrathiol and triallyl monomers mixed in a molar ratio of 100:125 (thiol:allyl functional groups), but without photoinitiator to facilitate straightforward OSTE-to-OSTE bonding[34] to the dielectric layer. In this work, the microchannel was first prepared by replica molding with the help of a PDMS mold, similar to previous work,[35] and then bonded to the dielectric layer. The microchannel featured a 38 mm long meandering channel (25 µm × 80 µm, $h \times w$) with ∅2 mm sample inlets/outlets, a double T injection cross (100 µm) for MCE, and 50 µm tapering (width) at the channel turns to prevent peak broadening.[44] The OSTE microchannels were fabricated by replica molding in three steps, including i) SU-8 master fabrication, ii) soft lithography of the poly(dimethyl siloxane) (PDMS) mold, and iii) replica molding of the OSTE channel.

The SU-8 master was fabricated from two layers of SU-8. The first layer was made of SU-8 100 by spreading (800 rpm, 45 s) and spin-coating (1200 rpm, 30 s) ≈200 µm thick layer on a 100 mm single side polished silicon wafer. Next, the SU-8 layer was soft-baked (65 °C for 25 min and 95 °C for 90 min) and UV exposed in contact mode for 10 s (Dymax 5000-EC flood exposure lamp, Dymax Corporation, Torrington, CT, nominal intensity 225 mW cm^{-2}) using a plastic mask to define the microchannel inlets. The second layer was made of SU-8 25 by spin-coating (2200 rpm, 30 s) ≈25 µm thick layer on top of the first SU-8 layer, followed by soft (65 °C for 3 min and 95 °C for 7 min), UV exposure for 3 s to define the microchannel, and postexposure bake of both layers at 65 °C for 8 min and at 95 °C for 20 min. The SU-8 layers were then developed in SU-8 developer for ≈20 min, rinsed with isopropanol, and dried in a nitrogen stream.

The PDMS mold was made from Sylgard 184 elastomer mixed with the curing agent in a ratio of 10:1 (w/w), degassed in vacuum, poured on the SU-8 master, cured in the oven (70 °C, 3 h), and finally detached from the SU-8 master. The tetrathiol and triallyl monomers were mixed in a molar ratio of 100:125 (thiol/allyl functional groups), degassed in vacuum, poured on the PDMS mold to yield ≈1 mm thick OSTE layer, and cured by UV for 4 min (Dymax 5000-EC). After curing, the OSTE replica was gently detached from the PDMS mold and bonded with the OSTE dielectric layer following preheating of both parts of the device to 70 °C. The OSTE-to-OSTE bond was finalized by curing under UV for 2 min (Dymax, flood exposure). Lastly, hydrophobic barriers were drawn around the microchannel inlets and outlets using molten beeswax to avoid buffer spreading over the relatively hydrophilic OSTE surface. Fully assembled devices (Figure 1d) were prepared by joining the DMF top plate with the bottom plate, incorporating the bonded microchannel, using two layers of double-sided tape (resulting in a gap of 200 µm) such that unit droplets (i.e., droplets covering a single driving electrode) had a volume of 1.3 µL. The top plate was assembled such that the flexible ITO-PET cover was resting on top of the sample inlet of the OSTE microchannel (Figure 1d). During DMF actuation, the top plate was grounded with the help of conductive tape sandwiched between the top and bottom plate. To facilitate application of the high voltage for electric-field driven flow in the OSTE microchannel, the contact pads of the microchannel electrodes were covered with conductive copper tape (conductive also through the adhesive).

Characterization of Thiol–Ene Dielectric Layer: 3D profiles of the spin-coated surfaces were acquired with a Profilm 3D optical profilometer (Filmetrics, San Diego, CA) equipped with a 20× objective. To illustrate a larger measurement area, four contiguous scans were stitched in ProfilmOnline software. For dielectric performance characterization, the devices were interfaced through pogo-pin connectors to an open-source DropBot v2.1 controller.[2] Electrodes were switched using solid-state relays and droplet velocities were measured using the open-source DropBot impedance-based feedback circuit as reported previously.[12,37] Droplets were actuated by applying a width normalized force of ≈25–30 µN mm^{-1} in a preprogrammed sequence. Unit droplets of water supplemented with 0.1% Tetronic 90R4 were actuated back and forth between adjacent electrodes. In each experiment, the electrostatic driving force applied to the droplet was increased in 2.5 µN mm^{-1} steps after each pair of droplet movements and at each step the resulting peak velocity was measured by DropBot as reported previously.[12,37] At least three droplets were evaluated on separate devices for each condition evaluated. Longevity tests were conducted by actuating droplets in a circular path for 10 min with a normalized force of 25 µN mm^{-1} in a preprogrammed sequence. At each step, the resulting peak velocity was measured by DropBot.

Droplet Transfer and Characterization of the Bonding Strength: Droplet transfer from DMF part of the device to the microchannel inlet was performed by actuating a sequence of electrodes so that a droplet was positioned on the feeding electrode. The bonding quality between the dielectric and the microchannel layers was ensured with the help of MCE, the signal (peak shape) of which is known to be sensitive to microchannel defects such as interlayer leakage. For

this purpose, the microchannel was filled with sodium borate buffer (20×10^{-3} M, pH 10) containing 0.1% SDS using vacuum suction. Before MCE runs, the integrated DMF–microchannel device was placed on the sample stage of an upright epifluorescence microscope (Zeiss Axioscope, Carl Zeiss AG, Oberkochen, Germany) together with the pogo-pin connector of the DropBot system. The HV was applied to the copper-covered contact pads of the microchannel electrodes using a custom-built programmable HV power supply (DC) and alligator clips. A typical MCE sequence comprised of an injection step (400 V cm^{-1}, 20 s) and separation step (750 V cm^{-1}). Fluorescence detection of the injected sample was performed at an effective separation length of 33 mm downstream from the injection cross, using HAL100 halogen lamp (Zeiss) equipped with a bandpass filter of 488 ± 5 nm as the excitation source. Fluorescence emission (500–700 nm) was recorded with a photomultiplier tube (Hamamatsu R5929, Cairn Research, Faversham, UK) perpendicular to the channel through a detection slit of 100 μm × 300 μm.

Supporting Information

Supporting Information is available from the Wiley Online Library or from the author.

Acknowledgements

G.S., M.H., and C.D. contributed equally to this work. This work was financially supported by the European Research Council (ERC/FP7, Grant No. 311705/CUMTAS), the Academy of Finland (Grant Nos. 307464, 309608, and 314303), the University of Helsinki (UH) Research Foundation, and the Natural Sciences and Engineering Research Council of Canada (NSERC). Authors thank Sari Tähkä (Faculty of Pharmacy, UH) for help with the MCE. G.S. also thanks the Doctoral program in materials research and nanoscience, UH, for additional funding. A.R.W. thanks the Canada Research Chair (CRC) program for a CRC.

Conflict of Interest

The authors declare no conflict of interest.

Keywords

digital microfluidics, inkjet-printed electronics, lab-on-a-chip, off-stoichiometric thiol–enes, replica molding

Received: May 11, 2020
Revised: June 24, 2020
Published online: August 11, 2020

[1] K. Choi, A. H. C. Ng, R. Fobel, A. R. Wheeler, *Annu. Rev. Anal. Chem.* **2012**, *5*, 413.
[2] R. Fobel, C. Fobel, A. R. Wheeler, *Appl. Phys. Lett.* **2013**, *102*, 193513.
[3] B. Coelho, B. Veigas, E. Fortunato, R. Martins, H. Águas, R. Igreja, P. V. Baptista, *Sensors* **2017**, *17*, 1495.
[4] D. Witters, K. Knez, F. Ceyssens, R. Puers, J. Lammertyn, *Lab Chip* **2013**, *13*, 2047.
[5] M. D. M. Dryden, D. D. G. Rackus, M. H. Shamsi, A. R. Wheeler, *Anal. Chem.* **2013**, *85*, 8809.
[6] D. G. Rackus, M. D. M. Dryden, J. Lamanna, A. Zaragoza, B. Lam, S. O. Kelley, A. R. Wheeler, *Lab Chip* **2015**, *15*, 3776.
[7] Y. Yu, R. P. S. de Campos, S. Hong, D. L. Krastev, S. Sadanand, Y. Leung, A. R. Wheeler, *Microsyst. Nanoeng.* **2019**, *5*, 10.
[8] A. E. Kirby, N. M. Lafrenière, B. Seale, P. I. Hendricks, R. G. Cooks, A. R. Wheeler, *Anal. Chem.* **2014**, *86*, 6121.
[9] A. E. Kirby, A. R. Wheeler, *Lab Chip* **2013**, *13*, 2533.
[10] C. Liu, K. Choi, Y. Kang, J. Kim, C. Fobel, B. Seale, J. L. Campbell, T. R. Covey, A. R. Wheeler, *Anal. Chem.* **2015**, *87*, 11967.
[11] G. Sathyanarayanan, M. Haapala, T. Sikanen, *Micromachines* **2018**, *9*, 649.
[12] C. Dixon, A. H. C. Ng, R. Fobel, M. B. Miltenburg, A. R. Wheeler, *Lab Chip* **2016**, *16*, 4560.
[13] A. H. C. Ng, R. Fobel, C. Fobel, J. Lamanna, D. G. Rackus, A. Summers, C. Dixon, M. D. M. Dryden, C. Lam, M. Ho, N. S. Mufti, V. Lee, M. A. M. Asri, E. A. Sykes, M. D. Chamberlain, R. Joseph, M. Ope, H. M. Scobie, A. Knipes, P. A. Rota, N. Marano, P. M. Chege, M. Njuguna, R. Nzunza, N. Kisangau, J. Kiogora, M. Karuingi, J. W. Burton, P. Borus, E. Lam, A. R. Wheeler, *Sci. Transl. Med.* **2018**, *10*, eaar6076.
[14] R. S. Sista, A. E. Eckhardt, V. Srinivasan, M. G. Pollack, S. Palanki, V. K. Pamula, *Lab Chip* **2008**, *8*, 2188.
[15] G. Sathyanarayanan, M. Haapala, I. Kiiski, T. Sikanen, *Anal. Bioanal. Chem.* **2018**, *410*, 6677.
[16] I. Barbulovic-Nad, H. Yang, P. S. Park, A. R. Wheeler, *Lab Chip* **2008**, *8*, 519.
[17] Y.-H. Chang, G.-B. Lee, F.-C. Huang, Y.-Y. Chen, J.-L. Lin, *Biomed. Microdevices* **2006**, *8*, 215.
[18] S. H. Au, M. D. Chamberlain, S. Mahesh, M. V. Sefton, A. R. Wheeler, *Lab Chip* **2014**, *14*, 3290.
[19] N. A. Mousa, M. J. Jebrail, H. Yang, M. Abdelgawad, P. Metalnikov, J. Chen, A. R. Wheeler, R. F. Casper, *Sci. Transl. Med.* **2009**, *1*, 1ra2.
[20] S. M. Kenyon, M. M. Meighan, M. A. Hayes, *Electrophoresis* **2011**, *32*, 482.
[21] A. Kecskemeti, A. Gaspar, *Anal. Chim. Acta* **2018**, *1021*, 1.
[22] R. Wu, L. Hu, F. Wang, M. Ye, H. Zou, *J. Chromatogr. A* **2008**, *1184*, 369.
[23] J. Gong, C.-J. Kim, *J. Microelectromech. Syst.* **2008**, *17*, 257.
[24] M. W. L. Watson, M. Abdelgawad, G. Ye, N. Yonson, J. Trottier, A. R. Wheeler, *Anal. Chem.* **2006**, *78*, 7877.
[25] M. Abdelgawad, M. W. L. Watson, A. R. Wheeler, *Lab Chip* **2009**, *9*, 1046.
[26] S. C. C. Shih, G. Goyal, P. W. Kim, N. Koutsoubelis, J. D. Keasling, P. D. Adams, N. J. Hillson, A. K. Singh, *ACS Synth. Biol.* **2015**, *4*, 1151.
[27] M. W. L. Watson, M. J. Jebrail, A. R. Wheeler, *Anal. Chem.* **2010**, *82*, 6680.
[28] F. Ahmadi, K. Samlali, P. Q. N. Vo, S. C. C. Shih, *Lab Chip* **2019**, *19*, 524.
[29] N. Kooy, K. Mohamed, K. Ibrahim, *J. Eng. Sci.* **2013**, *9*, 71.
[30] S. Tuomikoski, S. Franssila, *Sens. Actuators, A* **2005**, *120*, 408.
[31] S. Aura, T. Sikanen, T. Kotiaho, S. Franssila, *Sens. Actuators, B* **2008**, *132*, 397.
[32] M. Abdelgawad, A. R. Wheeler, *Microfluid. Nanofluid.* **2008**, *4*, 349.
[33] L. Mats, A. Bramwell, J. Dupont, G. Liu, R. Oleschuk, *Microelectron. Eng.* **2015**, *148*, 91.
[34] T. M. Sikanen, J. P. Lafleur, M.-E. Moilanen, G. Zhuang, T. G. Jensen, J. P. Kutter, *J. Micromech. Microeng.* **2013**, *23*, 037002.
[35] S. M. Tähkä, A. Bonabi, M.-E. Nordberg, M. Kanerva, V. P. Jokinen, T. M. Sikanen, *J. Chromatogr. A* **2015**, *1426*, 233.
[36] J. M. Ko, Y. H. Kang, C. Lee, S. Y. Cho, *J. Mater. Chem. C* **2013**, *1*, 3091.
[37] I. Swyer, R. Fobel, A. R. Wheeler, *Langmuir* **2019**, *35*, 5342.
[38] S.-J. Ding, P.-F. Wang, D. W. Zhang, J.-T. Wang, W. W. Lee, *Mater. Lett.* **2001**, *49*, 154.

[39] I. A. Lobo, P. A. Robertson, L. Villani, D. J. D. Wilson, E. G. Robertson, *J. Phys. Chem. A* **2018**, *122*, 7171.
[40] J. P. Lafleur, S. Senkbeil, J. Novotny, G. Nys, N. Bøgelund, K. D. Rand, F. Foret, J. P. Kutter, *Lab Chip* **2015**, *15*, 2162.
[41] J. P. Lafleur, R. Kwapiszewski, T. G. Jensen, J. P. Kutter, *Analyst* **2013**, *138*, 845.
[42] C. Fredrik Carlborg, T. Haraldsson, K. Öberg, M. Malkoch, W. van der Wijngaart, *Lab Chip* **2011**, *11*, 3136.
[43] S. Senkbeil, J. Aho, L. Yde, L. R. Lindvold, J. F. Stensborg, J. Rantanen, J. P. Lafleur, J. P. Kutter, *J. Micromech. Microeng.* **2016**, *26*, 075014.
[44] C.-H. Tsai, C.-H. Tai, L.-M. Fu, F.-B. Wu, *J. Micromech. Microeng.* **2005**, *15*, 377.